Networks of Limited-Valency Patchy Particles

P. J. M. Swinkels and R. Sinaasappel
Institute of Physics, University of Amsterdam, 1098XH Amsterdam, The Netherlands

Z. Gong and S. Sacanna
Molecular Design Institute, Department of Chemistry, New York University, New York, NY 10003-6688, USA

W. V. Meyer
Universities Space Research Association, with GEARS, NASA Glenn Research Center, 2001 Aerospace Parkway, Brook Park, Ohio 44152, USA

Francesco Sciortino
Department of Physics, University of Rome La Sapienza, 00185 Rome, Italy

P. Schall
Institute of Physics, University of Amsterdam, 1098XH Amsterdam, The Netherlands

(Received 6 June 2023; revised 27 November 2023; accepted 17 January 2024; published 16 February 2024)

Equilibrium gels provide physically attractive counterparts of nonequilibrium gels, allowing statistical understanding and design of the equilibrium gel structure. Here, we assemble two-dimensional equilibrium gels from limited-valency "patchy" colloidal particles and follow their evolution at the particle scale to elucidate cluster-size distributions and free energies. By finely adjusting the patch attraction with critical Casimir forces, we let a mixture of two-valent and pseudo-three-valent patchy particles approach the percolated network state through a set of equilibrium states. Comparing this equilibrium route with a deep quench, we find that both routes approach the percolated state via the same equilibrium states, revealing that the network topology is uniquely set by the particle bond angles, independent of the formation history. The limited-valency system follows percolation theory remarkably well, approaching the percolation point with the expected universal exponents.

DOI: 10.1103/PhysRevLett.132.078203

Load-bearing, space-spanning networks known as gels lend a wide range of common materials their rigidity. Colloidal gels typically form by an out-of-equilibrium process after the system becomes thermodynamically unstable, for example, as a result of a change in pH or the addition of depletants [1]. The out-of-equilibrium process forming and arresting the structures sets the properties of the resulting material but is not well understood in conventional thermodynamics, and there is no theory encompassing the aggregation and structure formation processes in the different systems. Besides these nonequilibrium routes, an equilibrium route to gelation has been suggested based on computer simulations [2], which does not involve irreversible phase separation and glasslike kinetic arrest. In this scenario, the bonding particles evolve through equilibrium states in forming the stable percolated network and, hence, can be described by conventional thermodynamics and derived from a partition function that predicts all measurable quantities, such as the cluster-mass distribution [3]. An interesting case is the formation of an equilibrium gel [2,4,5] from anisotropic, patchy particles [6–8]: In these essentially attractive systems, the network topology is set by the valency of the particles dictating their bonding direction. In the case of a mixture of particles with two different valencies, simulations found that a combination of the Wertheim [9] and Flory-Stockmayer (FS) theory [10], used for modeling chemical gelation, provides a theoretical framework, able to predict cluster growth and cluster-mass distributions [2]. The topology of such an equilibrium gel network is then also very different from that of a conventional colloidal gel formed by an out-of-equilibrium, arrest process. A system of primarily two-patch and a small fraction of higher-valency particles will tend to form single-particle filaments with branching points, in contrast to conventional colloidal gels, where thicker strands are common. The equilibrium gel state is also not expected to age [2]; even in the case of ongoing rearrangements, the network continues in an identical state, as there is no driving force for the network to tend to a more compact configuration.

While extensively studied in simulations, including a wide variety of patch numbers and mixtures of different valency particles [11–14], experimental studies have remained scarce; this has been—with a few exceptions [4,15–17]—due to the challenge of fabricating limited-valency particles

with finely adjustable interactions to sample equilibrium configurations. Therefore, direct particle-scale observation of equilibrium gels in experiments to test the applicability of Flory-Stockmayer theory have been challenging. Especially in two dimensions, where loops not included in the theory are ubiquitous, experimental verification has remained elusive.

Here, we assemble equilibrium networks from divalent and pseudo-trivalent colloidal particles to directly observe the formation of equilibrium networks using optical microscopy. We employ finely tunable critical Casimir interactions [18–21] to assemble networks via near-equilibrium and quench routes and elucidate the network properties and formation dynamics. By comparing the quench and near-equilibrium routes to percolation, we show that both lead through the same equilibrium states, demonstrating that the system evolves via a sequence of equilibrium configurations, even when a fast quench is applied. We find that the limited-valency system follows percolation theory remarkably well, approaching the percolation point with the expected universal exponents. Using the measured cluster-size distributions, we determine the free energy of the system and compare with Flory-Stockmayer theory predictions, adjusted to our two-dimensional system. These direct observations provide strong experimental evidence of the time-temperature correspondence in equilibrium gels.

We use two- and four-patch particles made by colloidal fusion [22,23], with diameters $d_{2p} = 3.2$ μm and $d_{4p} = 3.7$ μm, respectively, and patch sizes $\theta_{2p} = 21°$ and $\theta_{4p} = 17°$, with $\theta_{2/4p}$ the arc angle of the spherical patch, sufficiently small to allow only a single bond per patch. The particles are suspended in a binary mixture of 2,6-lutidine and water with lutidine volume fraction $c_L = 0.25$, just below the critical concentration $c_c = 0.30$ [24], in which they sediment. Upon addition of 1 mM magnesium sulfate, the patches develop an adsorption preference for lutidine, resulting in a tunable patch-to-patch attraction close to the solvent critical temperature $T_c = 33.86\,°\mathrm{C}$. We employ a two-patch to four-patch particle mixture with number ratio 6:1 and total surface fraction after sedimentation of $\eta \sim 0.1$. The patch-patch attraction is adjusted from $\sim 2k_BT$ to $> 15k_BT$ [23,25] by varying the temperature offset $\Delta T = T_c - T$ between 0.4 and 0.05 K. The particles' gravitational length is approximately $0.1d_{2p}$, confining them to the sample wall and leading to partial screening of the particles' bonding sites [26,32]: Upon free rotation, divalent particles become partially unavailable for bonding. When computing bond probabilities, as discussed in Supplemental Material [26], we account for this effect by assuming a fraction ζ of nonbonded divalent particles to be inactive as well as for the presence of a small fraction ι of both dimer and tetramer particles, which are inactive due to synthesis limitations.

Two different assembly routes are explored: a deep quench, increasing particle attractions quickly by heating through the temperature interval ΔT within 5 min, and a near-equilibrium route, increasing attractions in small increments by heating in steps of 0.05 K, while waiting between 4 and 6 h at each step for equilibration. The time intervals are chosen for stability reasons so that six temperature steps fit within the maximum experimental acquisition time of about a day [26]. Besides this system, we investigated a broader range of systems with different particle densities, di-to-tetrapatch particle ratios, and quench depth and found that the conclusions are robust within the systems studied. Optical microscopy is used to image the resulting particle assembly in real time and to locate particle centers using particle tracking software [33]. Neighboring particles whose centers are separated by less than 4.0 μm $\sim 1.1d_{4p}$ for at least five consecutive frames (50 s) are considered bonded and connected into networks.

The quenched system shows a distinct network spanning the field of view after about 4 h; see Fig. 1(a) and online video [34]. Three structural motifs are observed: chains of dipatch particles (I), kinked chains (II), and branching points joining three chains (III), the latter two connected by a tetrapatch particle. Since branching points of four chains are not observed, we conclude that, under gravity, the tetrapatch particles can form a maximum of three bonds, while the fourth patch is unavailable due to the particles' small gravitational height. We therefore consider the particles quasitrivalent, leading to an initial average valency of $\langle f \rangle = 2.14$ [26].

The evolution of particle clusters shows the emergence of a percolated state in Figs. 1(b)–1(d), where particle color indicates the number of bonded neighbors of a particle. Initially, linear clusters form, and, as the assembly evolves, the chains become increasingly cross-linked by pseudo-trivalent particles. This is reflected in the fractal dimension, which we determine by plotting the radius of gyration, r_g, as a function of the number of particles s in a cluster as shown in Figs. 1(e)–1(g). Initially, r_g grows linearly with the number of particles, resulting in a fractal dimension of $d_f = 1$ (dotted line), while for $s \gtrsim 10$ particles, the radius of gyration grows with a power of approximately 1.8^{-1}, indicating a fractal dimension of $d_f = 1.8$ (dashed line) [35]. The latter agrees with simulation results on similar limited-valency particles and is close to the percolation universality class value of $d_f = 91/48 \approx 1.89$, suggesting that percolation theory can be used to describe our system [13].

Unlike the quenched system, the near-equilibrium system shows frequent bond breaking, allowing the system to approach its equilibrium state at each step. To study the equilibration in more detail, we follow the second moment of the cluster-size distribution, $C = \sum s^2 N_s / \sum s N_s$, which provides a measure of the mean cluster size, in Fig. 2. Here, N_s is the number of clusters of size s. In the quenched case [Fig. 2(a)], C increases quickly and saturates after about 4 h. In contrast, along the near-equilibrium route [Fig. 2(b)], C displays stepwise growth, working toward a new equilibrium value at each interaction strength. This

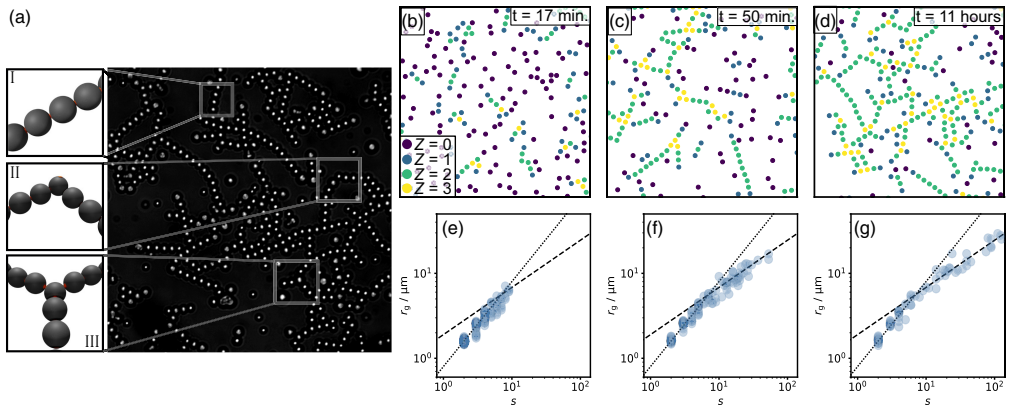

FIG. 1. Growth of colloidal network of divalent and pseudo-trivalent particles. (a) Optical microscope image of the network 9.75 h after quench to attractive strength $> 15k_BT$. Insets show reconstructions of three structural motifs: linear chains of dipatch particles (I), kinked chains (II), and branching point joining three chains (III), linked by a tetrapatch particle. A branching point with four chains is not observed. (b)–(d) Reconstructions showing the evolution of the particle network. Each dot represents a particle, and color indicates the number of bonded neighbors Z (see the legend). With time, a plane-spanning network emerges, where central trivalent hubs connect linear chains. (e)–(g) Radius of gyration r_g as a function of cluster size s for the snapshots in (b)–(d) showing the transition from linear chains with $r_g \propto s^1$ (dotted line) to a branched network with $r_g \propto s^{1/1.8}$ (dashed line), indicating a transition from fractal dimension $d_f = 1$ to fractal dimension $d_f = 1.8$.

trend is also reflected in the average number of bonds per particle $\langle Z \rangle$ indicated with hexagons in both panels (right axis). The quenched system shows a rapid increase to a plateau value, while the near-equilibrium system shows incremental approaches to intermediate $\langle Z \rangle$ values. Despite these differences, the eventually reached value of $\langle Z \rangle$ is remarkably similar: In both cases, saturation occurs at $\langle Z \rangle \approx 1.55$ at $\Delta T = 0.05$ K.

To investigate the scaling predictions of percolation theory, we plot the mean cluster size as a function of distance to the percolation point ($Z_c - \langle Z \rangle$) in Fig. 2(c), fixing Z_c to the theoretical value $Z_c = 1.875$ as explained in Supplemental Material [26].

Further away from Z_c, the mean cluster size increases with a power of ~2.1 for both routes, crossing over to an exponent of approximately 1 for the quench route at $Z_c - \langle Z \rangle \lesssim 0.3$. This scaling is in good agreement with the one expected from percolation theory: In a 2D system, C is expected to diverge with a critical exponent $\gamma = 43/18 \approx 2.4$, crossing over to 1 close to percolation [36]. The near-equilibrium route does not get close enough to percolation to observe this second scaling regime. The

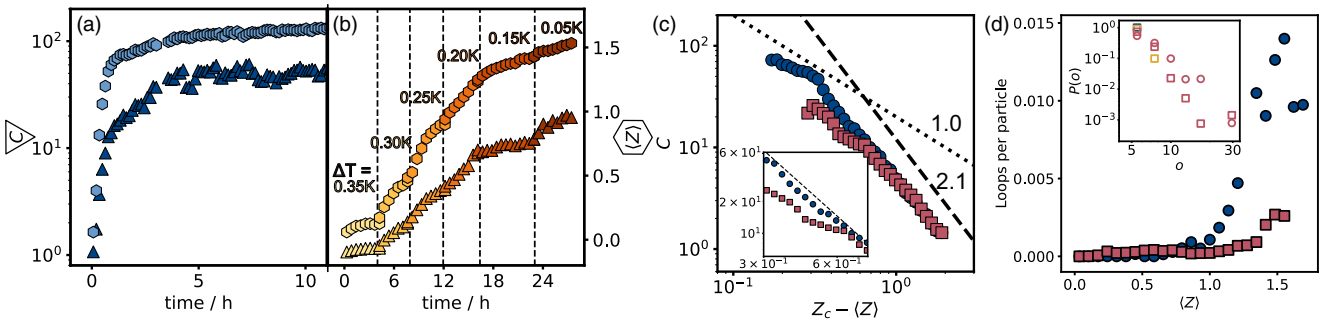

FIG. 2. Cluster evolution: quench and near-equilibrium routes. (a),(b) Cluster and bond evolution for the quench (a) and near-equilibrium route (b). Triangles indicate the second moment of the cluster-size distribution C (left y axis), and hexagons indicate the average number of bonds per particle $\langle Z \rangle$ (right y axis). In the near-equilibrium case (b), the temperature increments are indicated by vertical dashed lines and color grading. (c) Scaling of C with distance to the predicted percolation threshold (Z_c) for quench (blue dots) and near-equilibrium route (red squares). Lines indicate powers of 2.1 (dashed) and 1 (dotted). Inset: enlarged section enlarging the wobble around $Z_c - \langle Z \rangle \sim 0.6$. (d) Number of loops per particle as a function of $\langle Z \rangle$ for quench (blue dots) and near-equilibrium route (red squares). Inset: distributions of loop sizes o for increasing $\langle Z \rangle$, $\langle Z \rangle = 0.17$ (blue), 0.58 (yellow), and 1.13 (red) for quench (circles) and near-equilibrium route (squares). Loops larger than five particles exist only at later stages, i.e., for sufficiently large $\langle Z \rangle$; see [26] for details.

slight wobble at $Z_c - \langle Z \rangle \approx 0.6$ corresponding to $\langle Z \rangle \approx 1.2$ (see the inset for the enlarged section) coincides with the onset in the number of loops in the network, as shown in Fig. 2(d): While loops are absent at low coordination number, an abrupt increase is observed for $\langle Z \rangle \sim 1.2$–$1.3$, signaling a change in the network topology. This affects the cluster size: As closed loops saturate bonding sites that would otherwise be available for new particles to bind, the onset of loops is reflected in a decline of the growth of C. Besides this slight deviation in the critical scaling, the agreement with percolation theory is striking. We note that, unlike the similarity in the cluster critical scaling, the evolution of loops reveals an interesting quench dependence [Fig. 2(d)]: Initially, small five-membered loops form, starting at lower $\langle Z \rangle \sim 0.3$ along the equilibrium route, reflecting their finite formation time. Later, the quench route overtakes the equilibrium route, forming many more medium-size (5–12-membered) loops, as shown by the loop-size distribution in the inset and a detailed analysis in [26].

The similarity in the cluster critical scaling along the quench and near-equilibrium routes suggests that the systems proceed through the same aggregation states, uniquely defined by the number $\langle Z \rangle$ of bonds per particles. To elucidate this point, we plot cluster-size distributions for three distinct states $\langle Z \rangle$ in Fig. 3(a), where squares and circles indicate quench and equilibrium routes, respectively. Indeed, the data of both routes overlap almost perfectly, suggesting cluster properties do not depend on the formation history but only on the value of $\langle Z \rangle$. This is confirmed for all investigated particle densities and quench depth; see [26]. Large clusters become increasingly likely with increasing $\langle Z \rangle$; this is apparent from the right shift of the tails approaching a power law with exponent $\tau = 2.16$ close to percolation [black dotted line in Fig. 3(a)]. Percolation theory predicts that, close to percolation, the number of large clusters decreases as a power law with universal scaling constant in two dimensions $\tau = 187/91 \approx 2.05$ [36], which is in reasonable agreement with our experimental value. Some deviation is expected due to the inclusion of small clusters in the fit, for which the relation is not expected to hold, and the presence of loops in clusters. We furthermore show in Supplemental Material [26] that the cluster-size distribution of both routes can be described reasonably well by Flory-Stockmayer theory, despite the presence of loops, further supporting the equilibrium properties of the gels. We note that the out-of-plane rotation of unbonded dimer particles in our 2D geometry lowers their chance of binding and leads to an excess of monomers, which we have accounted for by a small correction of the FS model.

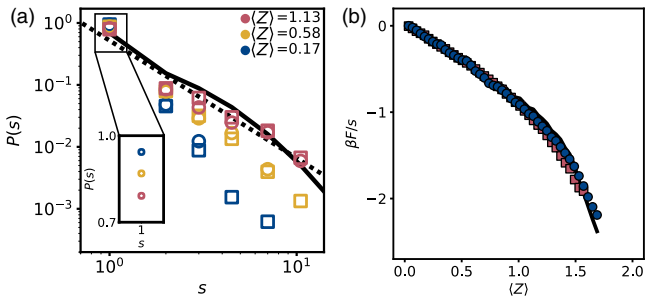

FIG. 3. Cluster-size distribution and free energy. (a) Cluster-size distributions for bond probabilities $\langle Z \rangle = 0.17$ (blue), 0.58 (yellow), and 1.13 (red) for the quench route (squares) and the near-equilibrium route (circles). The black dotted line indicates a power law with exponent $\tau = 2.16$. The black solid line shows the cluster-size distribution predicted by Flory-Stockmayer theory at $\langle Z \rangle = 1.13$; see Supplemental Material [26]. The inset shows the probability of free particles in the equilibrium case (quench omitted for clarity) with a linear y axis. (b) Helmholtz free energy per particle as a function of average number of bonds as determined from cluster-size distributions such as those in (a), for all stages of the experiment. The quench route (blue circles) and near-equilibrium route (red squares) as well as predictions from Flory-Stockmayer (solid black line; see Supplemental Material [26]) are all in good agreement. The free energy is determined using Eq. (1) and is solely dependent on the bonding state of the system.

Finally, we make use of the remarkable properties of equilibrium gels to relate the experimental cluster-size distribution to the free energy. Assuming that the system forms a two-dimensional ideal gas of clusters and that loops play a minor role, the Helmholtz free energy F can be expressed in terms of only the monomer concentration of both species and in terms of the total number of clusters [3,37] as

$$F/k_BT = N\mu_N/k_BT + L\mu_L/k_BT - \sum N_{n,l}, \qquad (1)$$

where N and L are, respectively, the number of trivalent and divalent particles, $N_{n,l}$ is the number of clusters consisting of n trivalent and l divalent particles, and $\mu_N/k_BT = \ln(N_{1,0}/A)$ and $\mu_L/k_BT = \ln(N_{0,1}/A)$ are, respectively, the chemical potentials of the trivalent and divalent monomers, with A the area [26]. We can, thus, use the measured cluster-size distributions from the quench and equilibrium routes, as well as the one predicted by Flory-Stockmayer theory [26], to determine the Helmholtz free energy as a function of $\langle Z \rangle$, as shown in Fig. 3(b). All three free energy curves overlap very well: The quench and near-equilibrium routes show almost identical free energies, which are both in close agreement with Flory-Stockmayer predictions (black solid line).

Our results confirm the existence of an equilibrium gel consisting of divalent and pseudo-trivalent particles experimentally: A slowly increasing attractive strength leads to the same network architecture as a quick quench. While the properties of conventional colloidal gels formed by kinetic arrest are strongly dependent on the formation history of

the gel, the limited-valency network experiences little to no dependence on its exact formation process and is rather determined by the valency and bond angles of the particles. Moreover, the structure of the system—quantified by its cluster-size distribution—is identical in quenched and near-equilibrium aggregation at equal $\langle Z \rangle$. This means that, during the kinetic process following the quench, the same configurations are sampled as in equilibrium when the total number of bonds is identical, providing the first experimental test of the time-temperature correspondence in equilibrium gels [38]. Fundamentally, this is due to the fact that the equilibrium state is time independent. Furthermore, despite the presence of loops and the difficulty of properly identifying a bond probability, Flory-Stockmayer theory can quantitatively describe the system when a small correction for the extra rotational degree of freedom of monomers in the pseudo-2D geometry is applied. A true three-dimensional system is challenging to achieve experimentally, but simulations show that the tetravalency of the tetrapatch particles reappears with growing gravitational height, as well as allowing 3D growth, leading to enhancement of larger clusters, and a progressive crossover of the cluster fractal dimension from the 2D to the 3D expected value; see [26]. Finally, we show that the free energy of the system can be directly inferred from the network state observed in experiments, made possible due to the equilibrium nature of our gel. Next to the powerful statistical mechanics description of these gels, our results highlight the architectural control and richness of patchy particle networks: By controlling the number ratio of divalent and pseudo-trivalent particles or the bonding angles, the network mesh size or local topology can be controlled, opening the door to designer colloidal networks and more general architectures.

[1] E. Zaccarelli, Colloidal gels: Equilibrium and non-equilibrium routes, J. Phys. Condens. Matter **19**, 323101 (2007).

[2] E. Bianchi, J. Largo, P. Tartaglia, E. Zaccarelli, and F. Sciortino, Phase diagram of patchy colloids: Towards empty liquids, Phys. Rev. Lett. **97**, 168301 (2006).

[3] F. Sciortino, Basic concepts in self-assembly, *Proceedings of the International School of Physics "Enrico Fermi", 193 (Soft Matter Self-Assembly)*, edited by edited by C. N. Likos, F. Sciortino, E. Zaccarelli, and P. Ziherl (IOS, Amsterdam; SIF, Bologna, 2016), pp. 1–17.

[4] S. Biffi, R. Cerbino, F. Bomboi, E. M. Paraboschi, R. Asselta, F. Sciortino, and T. Bellini, Phase behavior and critical activated dynamics of limited-valence DNA nanostars, Proc. Natl. Acad. Sci. U.S.A. **110**, 15633 (2013).

[5] E. Lattuada *et al.*, Spatially uniform dynamics in equilibrium colloidal gels, Sci. Adv. **7**, 49 (2021).

[6] S. C. Glotzer and M. J. Solomon, Anisotropy of building blocks and their assembly into complex structures, Nat. Mater. **6**, 557 (2007).

[7] E. Bianchi, R. Blaak, and C. N. Likos, Patchy colloids: State of the art and perspectives, Phys. Chem. Chem. Phys. **13**, 6397 (2011).

[8] Gi-Ra Yi, D. J. Pine, and S. Sacanna, Recent progress on patchy colloids and their self-assembly, J. Phys. Condens. Matter **25**, 193101 (2013).

[9] M. S. Wertheim, Fluids with highly directional attractive forces. IV. Equilibrium polymerization, J. Stat. Phys. **42**, 477 (1986).

[10] P. J. Flory, *Principles of Polymer Chemistry* (Cornell University Press, Ithaca and London, 1953).

[11] F. Sciortino, E. Bianchi, J. F. Douglas, and P. Tartaglia, Self-assembly of patchy particles into polymer chains: a parameter-free comparison between Wertheim theory and Monte Carlo simulation, J. Chem. Phys. **126**, 194903 (2007).

[12] D. de Las Heras, J. M. Tavares, and M. Telo da Gama, Soft matter, Soft Matter **12**, 5615 (2011).

[13] J. Russo, P. Tartaglia, and F. Sciortino, Association of limited valence patchy particles in two dimensions, Soft Matter **6**, 4229 (2010).

[14] G. Villar, A. W. Wilber, A. J. Williamson, P. Thiara, J. P. K. Doye, A. A. Louis, M. N. Jochum, A. C. F. Lewis, and E. D. Levy, Self-assembly and evolution of homomeric protein complexes, Phys. Rev. Lett. **102**, 118106 (2009).

[15] Q. Chen, S. C. Bae, and S. Granick, Directed self-assembly of a colloidal kagome lattice, Nature (London) **469**, 381 (2011).

[16] Q. Chen, E. Diesel, J. K. Whitmer, S. C. Bae, E. Luijten, and S. Granick, Triblock colloids for directed self-assembly, J. Am. Chem. Soc. **133**, 7725 (2011).

[17] M. He, J. P. Gales, É. Ducrot, Z. Gong, G.-R. Yi, S. Sacanna, and D. J. Pine, Colloidal diamond, Nature (London) **585**, 524 (2020).

[18] T. F. Mohry, S. Kondrat, A. Maciolek, and S. Dietrich, Critical Casimir interactions around the consolute point of a binary solvent, Soft Matter **10**, 5510 (2014).

[19] L. H. Nellen and C. Bechinger, Tunability of critical casimir interactions by boundary conditions, Europhys. Lett. **88**, 26001 (2009).

[20] F. Soyka, O. Zvyagolskaya, C. Hertlein, L. Helden, and C. Bechinger, Critical Casimir forces in colloidal suspensions on chemically patterned surfaces, Phys. Rev. Lett. **101**, 208301 (2008).

[21] S. Stuij, M. Labbe-Laurent, T. E. Kodger, A. Maciolek, and P. Schall, Critical Casimir interactions between colloids around the critical point of binary solvents, Soft Matter **13**, 5233 (2017).

[22] Z. Gong, T. Hueckel, G. R. Yi, and S. Sacanna, Patchy particles made by colloidal fusion, Nature (London) **550**, 234 (2017).

[23] S. Stuij, J. Rouwhorst, H. J. Jonas, N. Ruffino, Z. Gong, S. Sacanna, P. G. Bolhuis, and P. Schall, Revealing polymerization kinetics with colloidal dipatch particles, Phys. Rev. Lett. **127**, 108001 (2021).

[24] A. Stein, S. J. Davidson, J. C. Allegra, and G. F. Allen, Tracer diffusion and shear viscosity for the system 2,6-Lutidine-Water near the lower critical point, J. Chem. Phys. **56**, 6164 (1972).

[25] H. J. Jonas, S. G. Stuij, P. Schall, and P. G. Bolhuis, A temperature-dependent critical Casimir patchy particle model benchmarked onto experiment, J. Chem. Phys. **155**, 034902 (2021).

[26] See Supplemental Material at http://link.aps.org/supplemental/10.1103/PhysRevLett.132.078203 for details, which includes Refs. [27–31].
[27] J. Russo, P. Tartaglia, and F. Sciortino, Association of limited valence patchy particles in two dimensions, J. Phys. Condens. Matter **22**, 104108 (2010).
[28] P. Tartaglia and F. Sciortino, Association of limited valence patchy particles in two dimensions, Soft Matter **6**, 17 (2010).
[29] F. Sciortino and E. Zaccarelli, Equilibrium gels of limited valence colloids, Curr. Opin. Colloid Interface Sci. **30**, 90 (2017).
[30] P. J. M. Swinkels, S. G. Stuij, Z. Gong, H. Jonas, N. Ruffino, B. van der Linden, P. G. Bolhuis, S. Sacanna, S. Woutersen, and P. Schall, Revealing pseudorotation and ring-opening reactions in colloidal organic molecules, Nat. Commun. **12**, 2810 (2021).
[31] N. Kern and D. Frenkel, Fluid-fluid coexistence in colloidal systems with short-ranged strongly directional attraction, J. Chem. Phys. **118**, 9882 (2003).
[32] H. J. Jonas, P. Schall, and P. G. Bolhuis, Extended Wertheim theory predicts the anomalous chain length distributions of divalent patchy particles under extreme confinement, J. Chem. Phys. **157**, 094903 (2022).
[33] Daniel B. Allan, Thomas Caswell, Nathan C. Keim, Casper M. van der Wel, and Ruben W. Verweij, Soft- matter/trackpy: Trackpy v0.5.0. Zenodo repository, 2021.
[34] See time-lapse movie and description, https://www.youtube.com/watch?v=fONDJDyXA0Y.
[35] M. Muthukumar and H. Henning Winter, Fractal dimension of a crosslinking polymer at the gel point, Macromolecules **19**, 1284 (1986).
[36] D. Stauffer and A. Aharony, *Introduction to Percolation Theory*, rev. 2. ed. digital print edition (Taylor & Francis, London, 2003).
[37] Walter G. Chapman, George Jackson, and Keith E. Gubbins, Phase equilibria of associating fluids: Chain molecules with multiple bonding sites, Mol. Phys. **65**, 1057 (1988).
[38] S. Corezzi, C. De Michele, E. Zaccarelli, P. Tartaglia, and F. Sciortino, Connecting irreversible to reversible aggregation: Time and temperature, J. Phys. Chem. B **113**, 1233 (2009).